ESAIM: PROCEEDINGS AND SURVEYS, Vol. ?, 2019, 1-10
Editors: Will be set by the publisher

CELL MIGRATION IN COMPLEX ENVIRONMENTS: CHEMOTAXIS AND TOPOGRAPHICAL OBSTACLES

Alessandro Cucchi[1], Christèle Etchegaray[2], Nicolas Meunier[3], Laurent Navoret[4] and Lamis Sabbagh[5]

Abstract. Cell migration is a complex phenomenon that plays an important role in many biological processes. Our aim here is to build and study models of reduced complexity to describe some aspects of cell motility in tissues. Precisely, we study the impact of some biochemical and mechanical cues on the cell dynamics in a 2D framework. For that purpose, we model the cell as an active particle with a velocity solution to a particular Stochastic Differential Equation that describes the intracellular dynamics as well as the presence of some biochemical cues. In the 1D case, an asymptotic analysis puts to light a transition between migration dominated by the cell's internal activity and migration dominated by an external signal. In a second step, we use the contact algorithm introduced in [15, 18] to describe the cell dynamics in an environment with obstacles. In the 2D case, we study how a cell submitted to a constant directional force that mimics the action of chemoattractant, behaves in the presence of obstacles. We numerically observe the existence of a velocity value that the cell can not exceed even if the directional force intensity increases. We find that this threshold value depends on the number of obstacles. Our result confirms a result that was already observed in a discrete framework in [3, 4].

Introduction

Cell migration plays a central role in a wide variety of biological phenomena. In the immune system, leukocytes migrate into areas of injury where they mediate the immune response [6]. Migration of fibroblasts and vascular endothelial cells is crucial for wound healing [19]. In metastasis state, tumor cells migrate from the initial tumor mass into the circulatory system and then leave and migrate into other sites [2, 13]. Finally, cell migration is significant in many technological applications, such as tissue engineering, since it plays an important role in colonization of biomaterials scaffolding.

A striking feature of animal cells is their ability to polarize in response to environmental cues. This asymmetry is fundamental to the structure and function of most cell types. Front-rear polarization, characterized by the establishment of cell protrusive polarity and directed migration, is controlled by intrinsic cell properties but also by extracellular cues such as biochemical and physical cues. We will

[1] MAP5, Université Paris Descartes, Paris, France, *alessandro.cucchi@parisdescartes.fr*.

[2] INRIA, Institut de Mathématiques de Bordeaux, Bordeaux, France, *christele.etchegaray@inria.fr*.

[3] MAP5, Université Paris Descartes, Paris, & LaMME, Université Évry-Val d'Essonne, France, *nicolas.meunier@univ-evry.fr*.

[4] Institut de Recherche Mathématique Avancée, Université de Strasbourg, Strasbourg, France, *laurent.navoret@math.unistra.fr*

[5] Institut Montpelliérain Alexander Grothendieck, CNRS, Université de Montpellier, Montpellier, France, *lamissabbagh1992@gmail.com*.

focus here on the impact of biochemical and mechanical cues for cell crawling on a substrate. To do so we enrich the stochastic model introduced in [7], which describes cell crawling on an homogeneous substrate in the absence of any biochemical cues, to account for biochemical and mechanical cues. We first study the 1D case in the presence of a constant gradient of attractive signal in the medium, and we show that it captures different cell behaviours, namely a transition between migration dominated by the cell's internal activity and migration dominated by the external signal. More precisely, if the cell sensitivity to the signal is weak then the cell does not always follow the signal and it can go in another direction. On the contrary the cell follows the signal if its sensitivity to the signal is high. Then, we numerically investigate the additional role of physical constraints composed by topographical obstacles. This is done by considering the cell as a rigid disk in the spirit of [11] and by using a specific numerical method, introduced in [15, 18], to solve the problem of the contact with obstacles. We observe the existence of a velocity value that the cell can not exceed even if the directional force intensity increases. We find that this threshold value depends on the number of obstacles. It is to be noticed that such a result was already observed in [3, 4] for the case of a tracer particle that moves in a geometrically confined lattice system populated by bath particles moving randomly. We believe that this study could help to better understand some aspects of cell motility in tissues.

The plan of this paper is as follows: in Section 1 we describe the stochastic model we will use to describe crawling over a flat substrate in the presence of a constant gradient of external signal. In Section 2, we study the model in dimension one. Finally in Section 3, we enrich the model to account for obstacles.

1 A stochastic model for cell crawling in the presence of a constant gradient of attractive signal

1.1 A discrete stochastic jump process for cell activity

In this section, we enrich the model introduced in [9] that describes the cell crawling over a flat surface in the absence of external cue. We extend the model to take into account the effect of a constant gradient of attractive signal on the dynamics.

In the absence of external cue, cell crawling consists of four main stages (see Figure 1). At first, the cell extends protrusions in its direction of motion that adhere to the substrate and de-adhere at the cell rear. We distinguish two types of cell protrusion: lamellipodia that are wide and flat, and filopodia that are finger-like extensions. Finally, contractile forces generate at the rear of the cell pull the whole cell body forward.

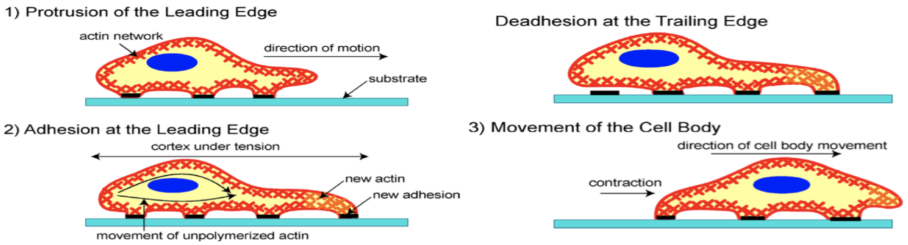

Figure 1. Scheme of cell crawling over a flat substrate [1]

We first recall the model introduced and studied in [7, 9, 10]. The cell is considered as a point, and the apparition/retraction of filopodial extensions are associated to forces acting on the cell dynamics (see Figure 2). Let N_t be the number of filopodia adhering on the substrate at time t, and denote by $\vec{V}_t$ and $(\vec{F}_i)_{i=1,\dots,N_t}$ respectively the cell velocity and the filopodial forces exerted by the filopodia at time t. Each filopodial force $\vec{F}_i$ is assumed to be unitary and constant in time. Denoting by $\theta_i = \arg(\vec{F}_i)$, $\theta_t = \arg(\vec{V}_t)$

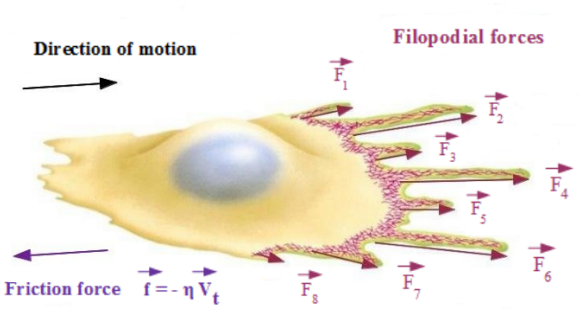

FIGURE 2. Scheme of a cell with the corresponding forces [16]

and $v_t = ||\vec{V}_t||$, the force and the velocity can be written in polar coordinates as $\vec{F}_i = (\cos\theta_i, \sin\theta_i)$ and $\vec{V}_t = (v_t, \theta_t)$. The cell motion with velocity $\vec{V}_t$ on the substrate leads to the appearance of a friction force which writes $\vec{f} = -\gamma\vec{V}_t$, where the parameter γ denotes the global friction substrate coefficient. Since the crawling of a cell on an adhesive substrate occurs at very small scales, the inertia is negligible for this system. Therefore by the force balance principle, the sum of the filopodial forces $(\vec{F}_i)_{i=1,\dots,N_t}$ and the friction $\vec{f}$ cancels leading to

$$\gamma\vec{V}_t = \sum_{i=1}^{N_t}(\cos\theta_i, \sin\theta_i). \tag{1}$$

Each filopodium is identified by the quantitative parameter $\theta \in [0, 2\pi)$ which indicates its orientation and one can introduce the Dirac measure δ_θ which characterizes each filopodium. In this framework, the set of all filopodial forces are described by the finite point measure ν_t defined by

$$\nu_t = \sum_{i=1}^{N_t}\delta_{\theta_i}.$$

For any measurable function f on $[0, 2\pi)$, the measure ν_t is such that $\langle\nu_t, f\rangle := \sum_{i=1}^{N_t} f(\theta_i)$ and $N_t = \langle\nu_t, 1\rangle$ corresponds to the filopodia population size. With this notation, Equation (1) translates into

$$\gamma\vec{V}_t = \big(\langle\nu_t, \cos\rangle, \langle\nu_t, \sin\rangle\big). \tag{2}$$

The Equation (2) represents the discrete model for computing the velocity $\vec{V}_t$ which is entirely described by the measure-valued jump process $(\nu_t)_t$. The events that rule the protrusion activity are the following:

- **Creation of filopodia**: new filopodia form with rate $c(\theta; \vec{V}_t)$, so that they form uniformly for a null velocity, and preferentially in the direction of motion when the velocity increases. This allows to model cell polarization. More precisely, the creation rate of filopodia is proportional to the probability density of a circular normal distribution centered in the direction of motion.
- **Individual death**: each filopodium may disappear with rate d.
- **Individual reproduction**: each filopodium is able to induce the formation of a new protrusion having the same orientation or a slightly modified orientation with reproduction rate r. In this latter case, the orientation of the new filopodium is chosen following a probability distribution $g(\cdot, \theta_i)$ assumed centered in the "parent's" orientation θ_i with constant variance.

The environment affects the cell migration either mechanically (i.e. rigidity and adhesiveness of the substrate, presence of obstacles,...) or chemically due to the presence of some molecular species which attract or repulse it. In both cases, the cell feels its outer environment by using molecular receptors located at its membrane and at protrusion tips. We consider now the situation where a constant gradient in attractive signal is present in the environment. We assume that the external signal causes the cell to polarize towards its source by inducing a constant bias in the protrusions activity. We enrich the model previously described by considering that the signal interferes with the creation of the protrusions and by taking into account the direction of the signal. Let θ_g be the angle pointing to the direction of the constant gradient of signal. A simple choice is to assume that the creation rate is proportional to a convex interpolation between the direction of cell motion θ_t and the direction of the signal θ_g:

$$c(\theta; \vec{V}_t, \theta_g) = c^* \left[(1-h) \frac{e^{\kappa(v_t)\cos(\theta-\theta_t)}}{2\pi I_0(\kappa(v_t))} + h \frac{e^{\beta\cos(\theta-\theta_g)}}{2\pi I_0(\beta)} \right], \tag{3}$$

where c^* is the spontaneous creation rate, $v_t = \|\vec{V}_t\|$, $\kappa(v_t) = \alpha v_t$ with $\alpha \geq 0$ representing the cell capacity to polarize i.e. to create protrusions in the direction of movement, the parameter $\beta \geq 0$ represents the cell sensitivity to the signal, I_0 denotes the 0-order modified Bessel function of first kind and $h \in [0,1]$ is a real number. We remark that for $h = 0$ we obtain the creation rate of the model of migration without signal introduced in [9]. It can be shown that these rates define a well-posed Markovian Jump process with values in the space of finite point measures on $[0, 2\pi)$ (see [8, 9, 12]).

1.2 A continuous stochastic model for cell crawling in the presence of a gradient of chemoattractants

As it was done in the absence of external signal [7,9], by using a rescaling procedure, by accelerating the dynamics and by considering infinitesimal filopodial forces, it is possible to derive a continuous migral model from the discrete one. In particular, it is possible to obtain the following Stochastic Differential Equation for the cell velocity $\vec{V}_t$:

$$d\vec{V}_t = \left[\frac{c}{\gamma} ((1-h)\tanh(\alpha v_t)\,\vec{e}_{\theta_t} + h\tanh(\beta)\,\vec{e}_{\theta_g}) - \lambda \vec{V}_t \right] \mathrm{d}t + \frac{\sigma}{\gamma}\,\mathrm{d}\vec{W}_t, \tag{4}$$

for $0 < t \leq T$ with $T < +\infty$. In Equation (4) $\lambda > 0$ is related to the lifetime of filopodia, $\sigma > 0$ quantifies the intensity of the noise, $\vec{e}_{\theta_t} = \vec{V}_t / v_t$ denotes the direction of the cell motion, $\vec{e}_{\theta_g}$ denotes the direction of the constant gradient of signal, and $(\vec{W}_t)_{t\geq 0}$ represents a given 2d standard Brownian motion. This equation has to be supplemented by a random initial velocity $\vec{V}_0$. We remark that when $h = 0$ we get

$$d\vec{V}_t = \left[\frac{c}{\gamma} \tanh(\alpha v_t) \vec{e}_{\theta_t} - \lambda \vec{V}_t \right] \mathrm{d}t + \frac{\sigma}{\gamma} \mathrm{d}\vec{W}_t. \tag{5}$$

Equation (5) was introduced in [8] as the continuous model to describe the cell crawling in the absence of signal. The first term in the right-hand side represents the capacity of the cell to polarize and to generate driving forces in the direction of motion. The second term accounts for a death term that originates in the discrete model from either protrusions retraction or the formation of protrusions in a direction antagonist to motion. Finally, the last term represents the stochastic fluctuations of the cell dynamics. When $\alpha = 0$, the model describes the dynamics of a passive particle moving by a damped Brownian motion. Whereas if $\alpha > 0$, the model takes into account the additional term related to the intracellular dynamics, namely the dynamics of the actin cytoskeleton and the capacity to polarize.

The aim of the next section is to study the different behaviors arising from the competition of the two phenomena, polarization vs external signal, when varying both parameters α and β.

2 A 1D continuous stochastic model for cell crawling in the presence of a gradient of chemoattractants

In this section we study equation (4) in dimension one. To do so we follow the lines of [9] in which equation (5) was studied in dimension one. The direction of the signal $\vec{e}_{\theta_g}$ becomes $+1$ if the signal is located on the positive side of the real line and -1 if it is located on the negative side. More precisely, we reach the following equation

$$\mathrm{d}V_t = \left[\frac{c}{\gamma}(1-h)\tanh(\alpha V_t) \pm h\frac{c}{\gamma}\tanh(\beta) - \lambda V_t\right]\mathrm{d}t + \frac{\sigma}{\gamma}\mathrm{d}W_t, \tag{6}$$

for $0 < t \leq T$. In this framework, the cell velocity V_t is a stochastic process taking values in $\mathbb{R}$ and W_t is the standard 1D-Brownian motion. In the first part of this section, we follow the lines of [9] and we recall how one can find the stationary distribution of V_t solving (6). In the second part we present the results of some numerical simulations.

Let $p_s(V,t)$ be the probability distribution of V_t. By Ito's formula, the density $p_s(V,t)$ solves the following Fokker-Planck partial differential equation

$$\partial_t\, p_s(V,t) = -\partial_V\left[f^{\pm}(V)\, p_s(V,t)\right] + \frac{\sigma^2}{2\gamma^2}\,\partial_V^2 p_s(V,t),$$

where

$$f^{\pm}(V) := \frac{c}{\gamma}(1-h)\tanh(\alpha V)\ \pm h\frac{c}{\gamma}\tanh(\beta) - \lambda V.$$

The stationary distribution $p_s(V)$ then satisfies the following equation

$$-\partial_V\left[f^{\pm}(V)\, p_s(V)\right] + \frac{\sigma^2}{2\gamma^2}\,\partial_V^2 p_s(V) = 0.$$

Integrating twice with respect to V, we get the explicit formulation for $p_s(V)$:

$$p_s(V) = \mathcal{N}\, e^{-W^{\pm}(V)}, \tag{7}$$

where $\mathcal{N}$ is a normalization constant and

$$W^{\pm}(V) := -\frac{2\gamma^2}{\sigma^2}\left((1-h)\frac{c}{\alpha\gamma}\ln(\cosh(\alpha V)) \pm h\frac{c}{\gamma}\tanh(\beta)V - \frac{\lambda}{2}V^2\right). \tag{8}$$

In order to study the different behaviours of the stationary velocity by varying the parameters α and β, one can look for the values of V that minimize the function $W^{\pm}$. Indeed by equation (7), the minima points of $W^{\pm}$ are also the maxima points of the stationary distribution p_s, and thus they represent the velocities which have the greatest probability to occur. In the following we consider the case for which the signal is on the negative side of the real line, and thus we analyze the function W^{-}.

Figure 3 shows the graph of the function W^{-} for $\beta = 0.1$ with $\alpha = 0.1$ (Figure 3a) and $\alpha = 10$ (Figure 3b). One can notice that for $\alpha = 0.1$ the function W^{-} has only one global minimum realized by $V \sim 0$. Instead, for $\alpha = 10$ there exist two minima points $V_1 < 0 < V_2$ for which W^{-} has a global minimum in V_1 and a local minimum in V_2. Therefore by considering $\beta = 0.1$, for $\alpha = 0.1$ the most probable velocity is $V \sim 0$ and the cell moves as a Brownian motion, whereas for $\alpha = 10$ there are two most probable velocities $V_1 < 0$ and $V_2 > 0$ but for which $W^{-}(V_1) < W^{-}(V_2)$ and the cell moves with more probability towards the signal.

Figure 4 shows the case for $\beta = 1$ with $\alpha = 0.1$ (Figure 4a) and $\alpha = 10$ (Figure 4b). One can notice that the function W^{-} has one global minimum for both $\alpha = 0.1$ and $\alpha = 10$ realized respectively by

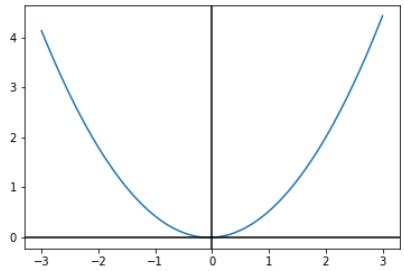

(A) $\alpha = 0.1$

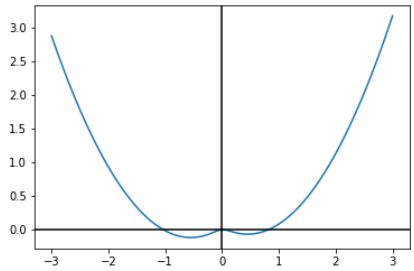

(B) $\alpha = 10$

FIGURE 3. Graph of the potential W^- defined by (8) for $h = 0.5$, $\lambda = 1$, $\gamma = c = \sigma = 1$, $\beta = 0.1$, $\alpha = 0.1$ (3a) and $\alpha = 10$ (3b).

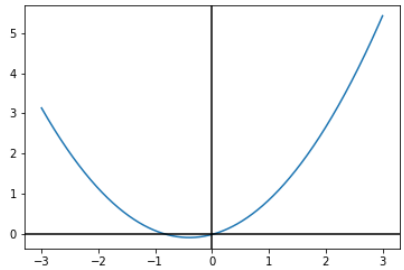

(A) $\alpha = 0.1$

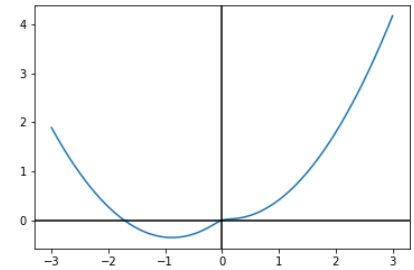

(B) $\alpha = 10$

FIGURE 4. Graph of the potential W^- defined by (8) for $h = 0.5$, $\lambda = 1$, $\gamma = c = \sigma = 1$, $\beta = 1$, $\alpha = 0.1$ (4a) and $\alpha = 10$ (4b).

$V_3 < 0$ and $V_4 < 0$ for which $V_3 < V_4$. This means that if $\beta = 1$ the cell moves towards the signal for both the values $\alpha = 0.1$ and $\alpha = 10$. In Figure 5 we show the graph of W^- with the same value $\beta = 1$ but for $\alpha = 100$. One can notice that in this case W^- has a global minimum for $V_5 < 0$ and a local minimum for $V_6 > 0$ such that $W^-(V_5) << W^-(V_6)$. Even if α is much more larger then the cases presented in Figure 4, the signal is strong enough to be picked up by the cell which then moves towards the signal.

2.1 Numerical simulations

In this section we perform some numerical simulations of Equation (6). We consider $h = 0.5$, $\lambda = 1$, $\gamma = c = \sigma = 1$ and the signal located in the negative side. We set $T = 1000$ and let $dt = 0.01$ be the time-step in the time interval $[0, 1000]$, and let $I = T/dt = 10000$ be the number of time iterations in $[0, 1000]$. For $n = 0, ..., I-1$ let $V^n = V(t^n)$ be the velocity at time $t^n := n \times dt$. We consider the initial condition $V^0 = 0$ and we compute the velocity V^{n+1} by using the Euler-Maruyama Method (see [14]) as follows:

$$V^{n+1} = V^n + \left[\frac{c}{2\gamma}\tanh(\alpha V^n) \pm \frac{c}{2\gamma}\tanh(\beta) - \lambda V^n\right] dt + \frac{\sigma}{\gamma} dW_n. \tag{9}$$

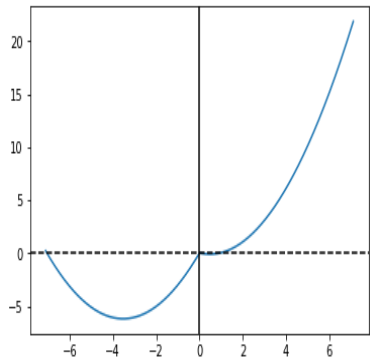

FIGURE 5. Graph of the potential W^- defined by (8) $h = 0.5$, $\lambda = 1$, $\gamma = c = \sigma = 1$, $\beta = 1$ and $\alpha = 100$.

Figures 6a and 6b show respectively the velocity histogram and the cell trajectory for $\beta = 0.1$ and $\alpha = 0.1$. We notice that the most probable velocity is around zero and that the cell moves as a Brownian particle. This is in agreement with the graph of W^- presented in Figure 3a.

Figures 6c and 6d show respectively the velocity histogram and the cell trajectory for $\beta = 0.1$ and $\alpha = 10$. We notice that there exist two most probable velocities, one strictly positive and the other strictly negative. We observe then that the cell moves with non-zero mean velocity by showing more persistence in the trajectory with respect to the Figure 6b.

Figures 7a and 7b show respectively the velocity histogram and the cell trajectory for $\beta = 1$ and $\alpha = 0.1$. The velocity histogram has a single peak shifted towards the direction of the signal and the cell trajectory show a strong persistence in the direction of the signal. This is in agreement with the graph of W^- presented in Figure 4a.

Figures 7c and 7d show respectively the velocity histogram and the cell trajectory for $\beta = 1$ and $\alpha = 10$. We observe that the velocity histogram does not have a unimodal shape but its larger peak is in the direction of motion. In addition, the cell trajectory has the same qualitative behavior of the one presented in Figure 7b.

Therefore, it seems that the cell may not follow the signal and go into the wrong direction if β is small and α is big, whereas when β is big the cell follows the signal if α is small and it may escape if α is big.

3 The effect of topographical obstacles on the cell dynamics

In this section, we study numerically the behavior of an active particle, with the previously described dynamics, in an environment containing obstacles and chemoattractants. In our framework, we consider one single moving particle in an environment containing a uniform distribution of fixed circular obstacles, where a constant gradient in signal induces a directional bias in its displacement.

We consider N uniformly distributed circular obstacles, each of center $q_i \in \mathbb{R}^2$ and radius $r_O > 0$. We also assume the cell to be a disk of center $X = X_t \in \mathbb{R}^2$ and radius $r > 0$. Let $T < +\infty$ and $t \in [0, T]$. As in the previous section, we denote by $\vec{V}_t \in \mathbb{R}^2$ the particle velocity at time t. In the absence of obstacles, the velocity $\vec{V}_t$ is solution of Equation (4). To deal with the presence of obstacles, that equation is complemented with a non-overlapping constraint. In particular, we use the method introduced in [15,18] which was developed for the case of a set of N moving particles. In the following, we give the main ideas of this framework and its numerical treatment. Finally, we show some numerical simulations.

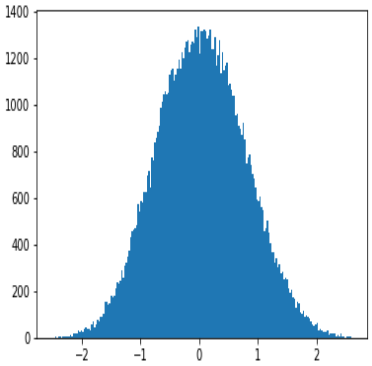

(A) Velocity histogram for $\alpha = 0.1$

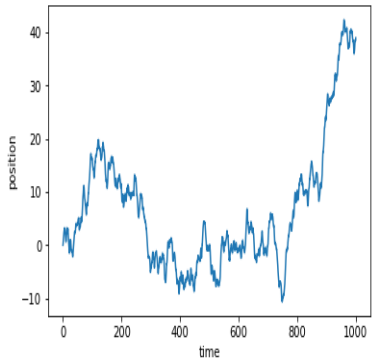

(B) Trajectory for $\alpha = 0.1$

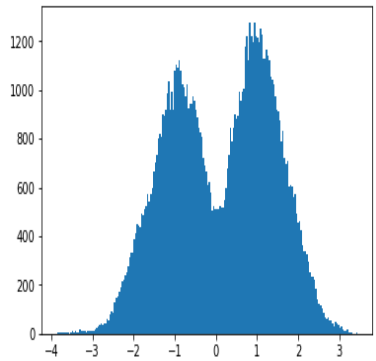

(C) Velocity histogram for $\alpha = 10$

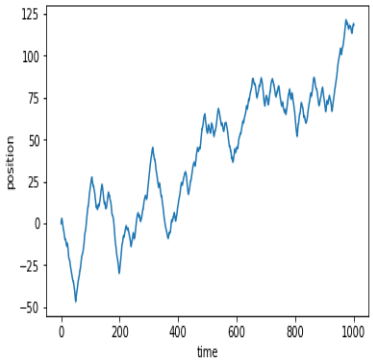

(D) Trajectory for $\alpha = 10$

FIGURE 6. Histogram for the velocity V solution of Equation (6) (6a,6c) and cell trajectory (6b,6d) for $h = 0.5$, $\lambda = 1$, $\gamma = c = \sigma = 1$, $\beta = 0.1$, $\alpha = 0.1$ (6a,6b) and $\alpha = 10$ (6c,6d).

3.1 Contact algorithm to deal with the obstacles

In this section we recall the contact algorithm presented in [15], that is meant to deal with the non-overlapping constraint. In the following we indicate by $V = V_t = \vec{V}_t$ the particle velocity and we use the notations of [15]. In particular, V is called spontaneous velocity, since it is the natural velocity which describes the particle's free motion. Now, when the particle "meets" an obstacle, its velocity does need to be modified by the contact algorithm in order to avoid the overlapping situation. This defines a (unique) new velocity $\mathcal{V}$ which will be called actual velocity. This method is based on a projection of the spontaneous velocities onto a set of admissible velocities.

Let $\mathbf{q} = (X, q_1, \dots, q_N) \in \mathbb{R}^{2(N+1)}$ be the vector of positions and for $i = 1, ..., N$ let $D_i(\mathbf{q}) := ||q_i - X|| - r_O - r$ be the signed distance between the obstacle i and the particle. We require $\mathbf{q}$ to belong to the set of feasible configuration Q defined by

$$Q = \{\mathbf{q} \in \mathbb{R}^{2(N+1)},\ D_i(\mathbf{q}) \geq 0\ \ \forall i = 1, ..., N\}.$$

The contact between the particle and an obstacle occurs when $D_i(\mathbf{q}) = 0$ for some $i = 1, ..., N$. In that case the velocity V needs to be modified in order to satisfy the non-overlapping constraint. One can

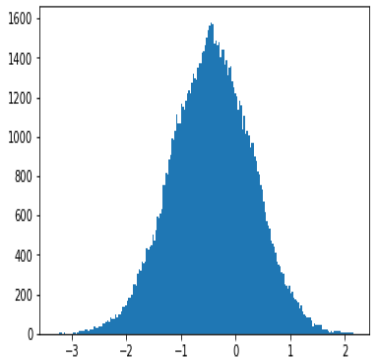

(A) Velocity Histogram for $\alpha = 0.1$

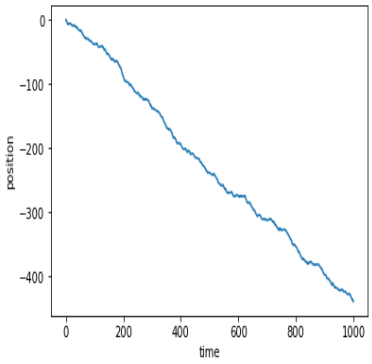

(B) Trajectory for $\alpha = 0.1$

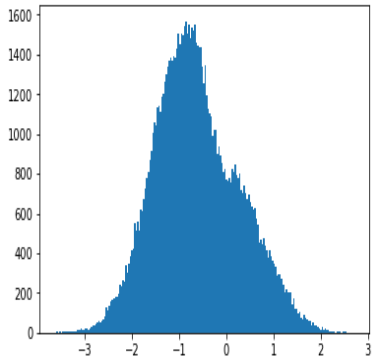

(C) Velocity Histogram for $\alpha = 10$

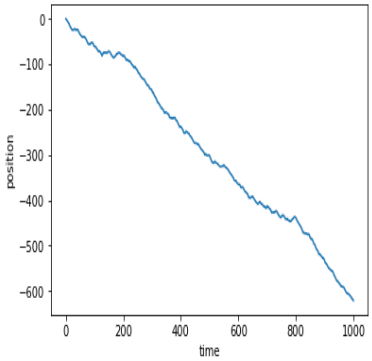

(D) Trajectory for $\alpha = 10$

FIGURE 7. Histogram for the velocity V solution of Equation (6) (7a,7c) and cell trajectory (7b,7d) for $h = 0.5$, $\lambda = 1$, $\gamma = c = \sigma = 1$, $\beta = 1$, $\alpha = 0.1$ (7a,7b) and $\alpha = 10$ (7c,7d).

introduce the set $\mathcal{C}_{\mathbf{q}}$ defined by

$$\begin{cases} \mathcal{C}_{\mathbf{q}} = \{v \in \mathbb{R}^2 : \text{ if } \ D_i(\mathbf{q}) = 0, \text{ then } \ G_i(\mathbf{q}) \cdot v \geq 0, \ \text{ for all } i = 1, ..., N\}, \\ G_i(\mathbf{q}) = e_i(\mathbf{q}) = \dfrac{X - q_i}{||X - q_i||} \in \mathbb{R}^2. \end{cases}$$

The quantity $G_i(\mathbf{q})$ indicates the normalized vector starting from q_i and pointing to X. If we denote by s the straight line passing through X and orthogonal to $G_i(\mathbf{q})$, the condition $G_i(\mathbf{q}) \cdot v \geq 0$ imposes that the particle's velocity v must belong to the half-space identified by the line s which does not contain the vector $G_i(\mathbf{q})$. Thus, the condition $G_i(\mathbf{q}) \cdot v \geq 0$ gives the admissible velocities v for which the non-overlapping constraint is verified. The actual velocity $\mathcal{V} \in \mathcal{C}_{\mathbf{q}}$ is defined as the admissible velocity which is the closest to V in the least square sense. Let $\mathrm{P}_{\mathcal{C}_{\mathbf{q}}} : \mathbb{R}^2 \to \mathcal{C}_{\mathbf{q}}$ be the projection operator of the spontaneous velocity space onto the admissible velocity space. Then $\mathcal{V}$ solves the following problem

$$\mathcal{V}_t = \mathrm{P}_{\mathcal{C}_{\mathbf{q}}}(V_t), \quad \text{for all } t \in (0, T]. \tag{10}$$

For the mathematical properties of the contact algorithm expressed by Equation (10), we refer to [15,18]. In the following, we recall the numerical method for solving Equation (10) introduced in [15].

3.2 Numerical scheme introduced in [15]

In this section, we recall the numerical scheme introduced in [15] to simulate the dynamics of a particle in interaction with topographical obstacles. In particular, in [15] it is shown that the approximation of $\mathcal{V}$ is also the solution of a minimization problem reformulated in a saddle-point form, whose resolution can be done by the Uzawa algorithm (see also [17]).

For fixed $T < +\infty$, we consider $[0, T]$ as the time interval. Let $I \in \mathbb{N}^*$ and $\delta := T/I$, we denote by $\{t^n := n\delta\}$ for $n = 1, ..., I$ the time discretization. Let $V^n := V_{t^n}$ and $\mathcal{V}^n := \mathcal{V}_{t^n}$, the quantity V^n is then obtained by the following rule

$$\begin{cases} \mathcal{V}^n = \mathrm{P}_{\mathcal{C}^\delta_{\mathbf{q}^n}}(V^n), \\ \mathcal{C}^\delta_{\mathbf{q}} = \{v \in \mathbb{R}^2,\ D_i(\mathbf{q}) + \delta\, G_i(\mathbf{q}) \cdot v \geq 0 \text{ for all } i = 1, ..., N\}. \end{cases} \tag{11}$$

The definition of $\mathcal{C}^\delta_{\mathbf{q}}$ is based on a first order approximation, in terms of velocity, of the non-overlapping constraint expressed in $\mathcal{C}_{\mathbf{q}}$. Let $U := V^n$, $\mathcal{U} := \mathcal{V}^n$, and $\mathcal{C}_{\mathbf{q}} := \mathcal{C}^\delta_{\mathbf{q}}$, we consider the functional J defined by $J(v) := ||v - U||^2$. The actual velocity $\mathcal{U}$ is solution of the following minimization problem under constraints

$$\begin{cases} \mathcal{U} \in \mathcal{C}_{\mathbf{q}}, \\ J(\mathcal{U}) = \min\limits_{v \in \mathcal{C}_{\mathbf{q}}} J(v). \end{cases} \tag{12}$$

Let $B : \mathbb{R}^2 \to \mathbb{R}^N$ be the operator defined by

$$Bv := (B_1 v, ..., B_N v) \ \text{ where } \ B_i v := -\delta\, G_i(\mathbf{q}) \cdot v.$$

The set of constraints $\mathcal{C}_{\mathbf{q}}$ rewrites as follows

$$\mathcal{C}_{\mathbf{q}} = \{v \in \mathbb{R}^2 : Bv \leq D\}, \ \text{ where } D = D(\mathbf{q}) = (D_i(\mathbf{q}))_{i=1,...,N} \in \mathbb{R}^N.$$

Let C be the cone $\mathbb{R}^N_+$ and let $\mathcal{L} : \mathbb{R}^2 \times C \to \mathbb{R}$ be the Lagrangian associated to (12) defined by

$$\mathcal{L}(v, \mu) = J(v) + \mu \cdot (Bv - D).$$

Consider the following saddle-point problem

$$\begin{cases} (\mathcal{U}, \lambda) \in \mathbb{R}^2 \times C, \\ \mathcal{L}(\mathcal{U}, \mu) \leq \mathcal{L}(\mathcal{U}, \lambda) \leq \mathcal{L}(v, \lambda) \ \ \forall v \in \mathbb{R}^2, \forall \mu \in C. \end{cases} \tag{13}$$

One can remark that for the problem (13), the couple solution $(\mathcal{U}, \lambda)$ is such that $\mathcal{U}$ realizes the minimum of $\mathcal{L}$ among the velocities $v \in \mathbb{R}^2$ and λ realizes the maximum of $\mathcal{L}$ among the lagrangian multipliers $\mu \in C$. One can have the following properties.

Proposition 3.1 ([15]). *If the couple $(\mathcal{U}, \lambda)$ is solution of (13), then $\mathcal{U}$ is solution of (12).*

Proposition 3.2 ([15]). *The couple $(\mathcal{U}, \lambda)$ is solution of (13) if and only if the couple $(\mathcal{U}, \lambda)$ is solution of (14) defined by*

$$\begin{cases} \mathcal{U} + B^t\lambda = U, \\ B\mathcal{U} \leq D, \\ \lambda \cdot (B\mathcal{U} - D) = 0. \end{cases} \tag{14}$$

The interest is then to solve (14) numerically. To this aim, a possible choice is to use the Uzawa algorithm which generates two sequences (v_k, μ_k) according to the following rule

$$\begin{cases} \rho > 0, \ \ \mu_0 \in \ C, \\ v_k = U - B^t\mu_{k-1}, \\ \mu_k = \Pi_+(\mu_{k-1} + \rho\,[Bv_k - D]), \end{cases} \tag{15}$$

where Π_+ is the euclidean projection onto the cone C and ρ is a fixed parameter. The algorithm can be shown to converge as soon as $0 < \rho < 2/||B||^2$ see e.g. [5]. Under this hypothesis, one can get that μ_k converges to some λ and v_k converges to $\mathcal{U}$ such that the couple $(\mathcal{U}, \lambda)$ is solution of (14).

3.3 Numerical simulations

We present in this section some numerical simulations. We describe the geometry we use and a method for building the uniform distribution of obstacles and then we show some numerical results. We use in particular the following numerical method. We set $T = 50$ and let $dt = 0.05$ be the time-step in the time interval $[0, 50]$, and let $I = T/dt = 2000$ be the number of time iterations in $[0, 50]$. For $n = 0, ..., I-1$ let $V^n \in \mathbb{R}^2$ be the spontaneous velocity and $\mathcal{V}^n \in \mathbb{R}^2$ be the actual velocity at time $t^n = n \times dt$. We then write $V^n = (u^n, v^n)$ and $\mathcal{V}^n = (z^n, w^n)$ and we consider random initial conditions V^0 and $\mathcal{V}^0$. We first compute the velocity V^{n+1} by using the Euler-Maruyama Method (see [14]) for the Equation (4):

$$\begin{cases} u^{n+1} = z^n + \dfrac{c}{\gamma}\left[(1-h)\tanh(\alpha||\mathcal{V}^n||)\, e^x_{\theta_n} + h\tanh(\beta)\, e^x_{\theta_g} - \lambda z^n\right] dt + \dfrac{\sigma}{\gamma} dW^x_n, \\ v^{n+1} = w^n + \dfrac{c}{\gamma}\left[(1-h)\tanh(\alpha||\mathcal{V}^n||)\, e^y_{\theta_n} + h\tanh(\beta)\, e^y_{\theta_g} - \lambda w^n\right] dt + \dfrac{\sigma}{\gamma} dW^y_n, \end{cases}$$

where $\vec{e}_{\theta_n} = (e^x_{\theta_n}, e^y_{\theta_n})$ is the direction of the motion at time t^n, $\vec{e}_{\theta_g} = (e^x_{\theta_g}, e^y_{\theta_g})$ is the direction of the constant gradient of the signal and $dW_n = (dW^x_n, dW^y_n)$ indicates the 2D-Brownian motion at time t^n. Successively, we compute the velocity $\mathcal{V}^{n+1}$ by using the Uzawa algorithm described in (15). In particular, at step $k+1$ of the Uzawa algorithm we compute

$$\begin{cases} z^{n+1}_{k+1} = u^{n+1} - (\mu_k \cdot \mathbf{e}_1)\, dt, \\ w^{n+1}_{k+1} = v^{n+1} - (\mu_k \cdot \mathbf{e}_2)\, dt, \\ \mu_{k+1} = \Pi_+(\mu_k - \rho[\,(z^{n+1}_{k+1}\mathbf{e}_1 + w^{n+1}_{k+1}\mathbf{e}_2)\, dt - \mathbf{G}\,]) \end{cases}$$

with initial condition $\mu_0 = 0$ and $\rho > 0$, where $\mathbf{e}_1, \mathbf{e}_2 \in \mathbb{R}^N$ indicate respectively the normalized distance between the center of the particle and the centers of the obstacles along the x-axis and the y-axis and the vector $\mathbf{G} \in \mathbb{R}^N$ indicates the signed distance between the particle and the obstacles.

In the following, we simulate different cases. First, we investigate the effect of obstacles on the dynamics of a Brownian particle that may be damped by a friction term. Then, we additionally consider a constant directional force and its effect on the dynamics. Finally, we consider the full dynamics as described in

Equation (4), that accounts for cell dynamics. In particular, it provides some intrinsic persistence in the displacement, and we investigate its interaction with both the obstacles and the constant force. We remark that the constant force can describe the presence of a constant gradient in chemical signal in the environment of the particle.

3.3.1 Geometry and obstacles distribution

We start by describing the geometry of the domain and the obstacles distribution. We consider a domain $\Omega = [0, L] \times [0, H]$, for some $L, H > 0$ and an uniform obstacles distribution which depends on the dimensions of Ω. Let r_O and r be the obstacles radius and the cell radius respectively, and let N be the total number of obstacles in Ω. N is computed by the following rule. Let $\varepsilon > 0$ be a geometry parameter to assure the particle to pass between two obstacles and let $d = 2r_O + 2r + 2\varepsilon$ be the minimal distance between two obstacles to ensure the passage of the particle. Let N_1 and N_2 be the number of obstacles along the horizontal and vertical directions respectively, defined by

$$N_1 = \left[\frac{L}{d}\right] \text{ and } N_2 = \left[\frac{H}{d}\right],$$

where $[\,\cdot\,]$ indicates the integer part function. The total number of obstacles in the domain Ω is then

$$N = N_1 \times N_2.$$

We decide to fix the parameter $\varepsilon = 0.01$ and to consider $r = mr_O$ for some $m > 0$. In Figure 8 we show two examples of the geometry for a particular choice of the parameters.

In the following, we consider the domain $\Omega = [0, 2] \times [0, 2]$ for which we impose periodic boundary conditions on the particle's displacement. We consider different numbers of obstacles N by varying the obstacles radius r_O.

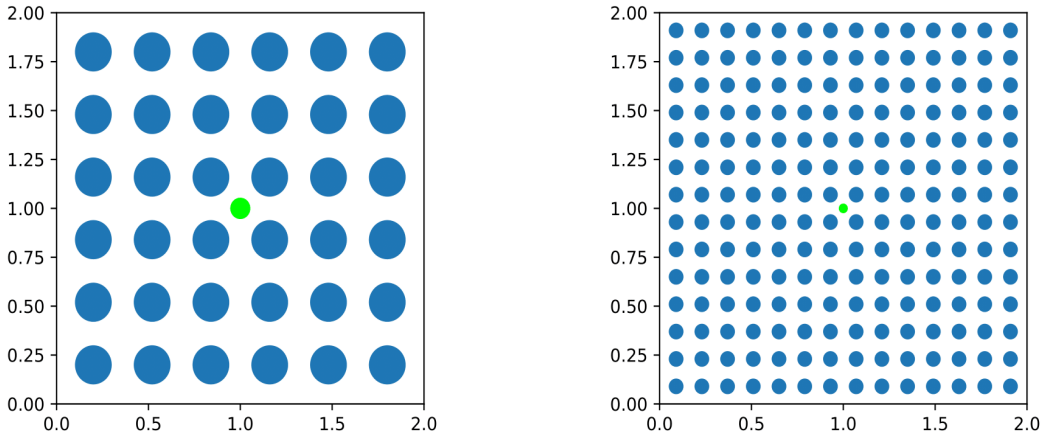

(A) $N = 36$ (B) $N = 900$

FIGURE 8. Domain $\Omega = [0, 2] \times [0, 2]$. Obstacles in blue, cell initial position in green. For case (a): $\varepsilon = 0.01$, $r_O = 0.1$, $r = r_O/2 = 0.05$. For case (b): $\varepsilon = 0.01$, $r_O = 0.04$, $r = r_O/2 = 0.02$.

3.3.2 Effect of obstacles on the dynamics of a Brownian particle

In this section, we consider the case of a particle moving according to a damped Brownian motion. In particular, we set $\alpha = 0, \beta = 0, \sigma = 1$ and we investigate the particle's dynamics for different values of $\lambda > 0$ and different numbers of obstacles.

In Figure 9, we show the one and two dimensional velocity histograms for $N = 36$ obstacles (Figures 9a-9c), and for $N = 900$ obstacles in (Figures 9d-9f). We first notice that the one dimensional velocity histograms are symmetric. This is due to the fact that there is not any bias in the particle's dynamics, and the obstacles are uniformly distributed in the domain. By analysing the two dimensional velocity histograms, we notice that the presence of obstacles does have an effect on the direction of the velocity. For $N = 36$, they show different shapes depending on the value of lambda. For $\lambda = 0$, the histogram has a squared shape, while it becomes more circular for larger values of λ. This shows that when the dynamics is weakly damped, the obstacles act on the directionality of the particle by preventing displacements in other directions than along the x and y axis. For $N = 900$, the 2D histograms have the same squared shape, but as λ increases, this shape becomes more smooth. In particular, we see that as the number of obstacles increases, the squared shape of the velocity histogram becomes more squared.

In Figure 10, we show two trajectories for $N = 900$ obstacles with $\lambda = 0$ (Figure 10a) and $\lambda = 3$ (Figure 10b). We notice that for $\lambda = 0$ we observe directional displacement in the particle's trajectory, which covers all the domain. For $\lambda = 3$, we observe a more compact trajectory, which mainly covers the upper-right part of the domain. This shows how the persistence induced by the obstacles is stronger for $\lambda = 0$ than for $\lambda = 3$.

3.3.3 Effect of a constant force on the dynamics of a Brownian particle

In this section, we study the effect of a constant directional force on a Brownian particle. In particular, we set $\alpha = 0$, $\lambda = 1$, $\sigma = 0.2$ and then we consider a normalized force $F = (2 \times 2/5, 1.5 \times 2/5)$. The parameter β describes the intensity of the effect of the force F on the particle's dynamics. We investigate the interplay between the force and the obstacles by varying β and the number of obstacles N.

Figure 11 shows the mean velocity modulus as a function of different values of β, for different numbers of obstacles. Since Equation (4) involves only $\tanh(\beta)$, we take $\beta \in [0, 10]$, as larger values do not change the dynamics. The mean velocity was obtained by simulating the model among $M = 100$ simulations. Figure 11 shows that the mean velocity modulus curve has a non-strictly-monotone behaviour with respect to β, for any number of obstacles. This is explained by the presence of the obstacles. For small values of β, the curve is monotonic-increasing when β increases. But when β is large enough, the curve reaches an horizontal asymptote. This is due to the fact that when the force intensity is strong enough, the particle gets stuck between the obstacles. We notice also that the mean velocity modulus decreases as the number of obstacles N increases. This shows how obstacles make the environment congested and prevent the particle's motion.

In Figure 12, we show the one and two dimensional velocity histograms for $N = 900$ obstacles with $\beta = 0.5$ (Figure 12a), $\beta = 2$ (Figure 12b) and $\beta = 6$ (Figure 12c). We first notice that the one dimensional histograms for x-component and y-component of the velocity show an asymmetry towards positive values, which is due to the bias induced by the force F. Since the x-component of the force is greater than its y-component, the asymmetry is stronger in the x-component of the velocity than in its y-component. For $\beta = 0.5$, the asymmetry is very weak and it becomes stronger as β increases. By analysing the two dimensional velocity histograms, we notice that the presence of the force makes the velocity distribution more concentrated toward the half-upper-right side of the domain. For $\beta = 0.5$, this effect is weak but remarkable. As β increases the effect becomes stronger and more remarkable. Figure 13 shows two particle's trajectories for $N = 900$ obstacles, for $\beta = 0.5$ (Figure 13a) and $\beta = 6$ (Figure 13a). We first notice that for both the cases, the particle's trajectory covers all the domain. For $\beta = 6$, the trajectory direction points toward the upper-right side of the domain, while for $\beta = 0.5$ the trajectory direction

$N = 36$

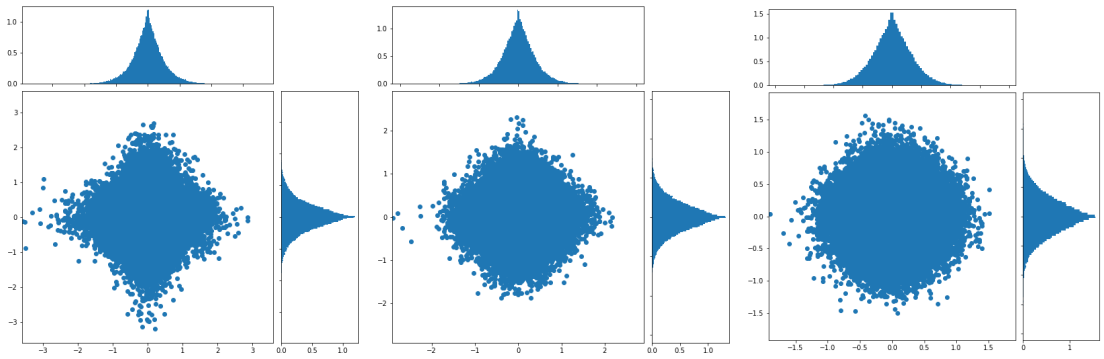

(A) $\lambda = 0$ (B) $\lambda = 1$ (C) $\lambda = 3$

$N = 900$

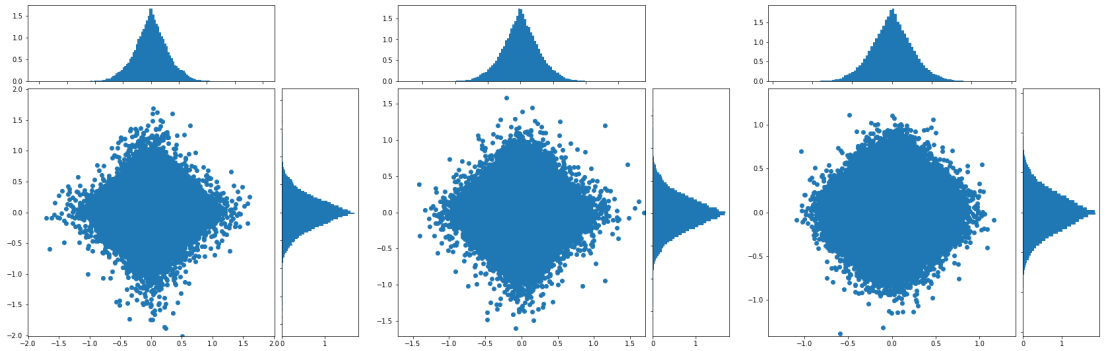

(D) $\lambda = 0$ (E) $\lambda = 1$ (F) $\lambda = 3$

FIGURE 9. One and two dimensional velocity histograms for $N = 36$ obstacles (9a-9c) and for $N = 900$ obstacles (9d-9f). Parameters: $\alpha = 0$, $\beta = 0$, $\sigma = 1$, $\lambda = 0$ (9a) and (9d), $\lambda = 1$ (9b) and (9e), $\lambda = 3$ (9c) and (9f).

changes more frequently. This is due to the fact that as β increases, the intensity of the effect of the force on the particle's dynamics becomes stronger.

3.3.4 Dynamics of an active particle with cellular dynamics

In this section, we study the effect of a constant directional force on an active particle for which the velocity is solution of equation (4) and mimics the dynamics of a cell. In particular, we set $\lambda = 1$, $\sigma = 0.2$ and we take the same force F as previously, namely $F = (2 \times 2/5, 1.5 \times 2/5)$. We perform similar numerical experiments as the ones done in the previous section, but now we consider $\alpha > 0$. The parameter α appears in the dynamics in (4) through the term $\tanh(\alpha v)$, where v indicates the norm of the velocity. To investigate the competition between the two parameters α and β, we focus on large values of α. In particular, in the following we consider $\alpha = 30$ and we let vary $\beta \in [0, 10]$.

Figure 14 shows the mean velocity modulus as a function of different values of β and for different numbers of obstacles, by setting $\alpha = 30$. In comparison with Figure 11, we notice that the qualitative

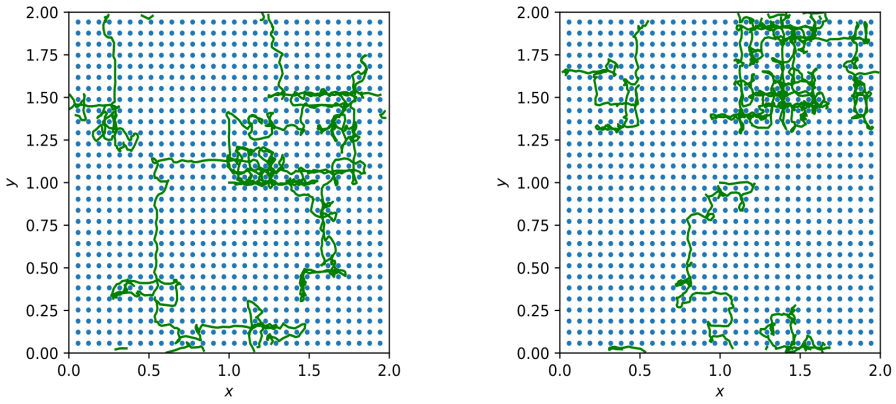

(A) $\lambda = 0$ (B) $\lambda = 3$

FIGURE 10. Particle's trajectories for $N = 900$ obstacles. Parameters: $\alpha = 0$, $\beta = 0$, $\sigma = 1$, $\lambda = 0$ (10a) and $\lambda = 3$ (10b).

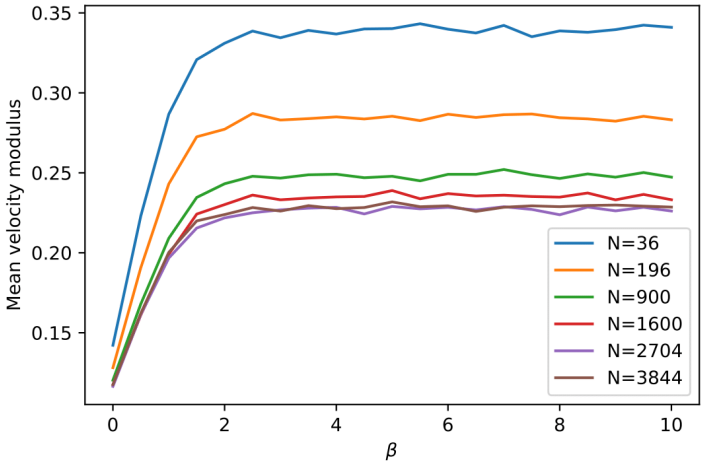

FIGURE 11. Mean velocity modulus among $M = 100$ simulations. We set $\alpha = 0$, $\lambda = 1$, $\sigma = 0.2$ and we simulated for 20 values of $\beta \in [0, 10]$. Numbers of obstacles considered: $36, 196, 900, 1600, 2704, 3844$.

behaviour of the mean velocity modulus does not change. We remark only that in Figure 14 the mean velocity modulus assumes smaller values with respect to the results presents in Figure 11.

In Figure 15, we show the one and two dimensional velocity histograms for $N = 900$ obstacles with $\beta = 0.5$ (Figure 15a), $\beta = 2$ (Figure 15b) and $\beta = 6$ (Figure 15c). We first notice that the one dimensional histograms for x-component and y-component of the velocity show a shift towards positive values, which is due to the bias induced by the force F. In comparison with the histograms in Figure 12, this asymmetry is less strong for both the x-component and the y-component. This is due to the fact that the internal dynamics intensity may play against the effect of the force. By analysing the two dimensional velocity histograms, we notice that in comparison with Figure 12, the velocity distribution is less squared and more concentrated in other other parts of the domain with respect to the half-upper-right side. For

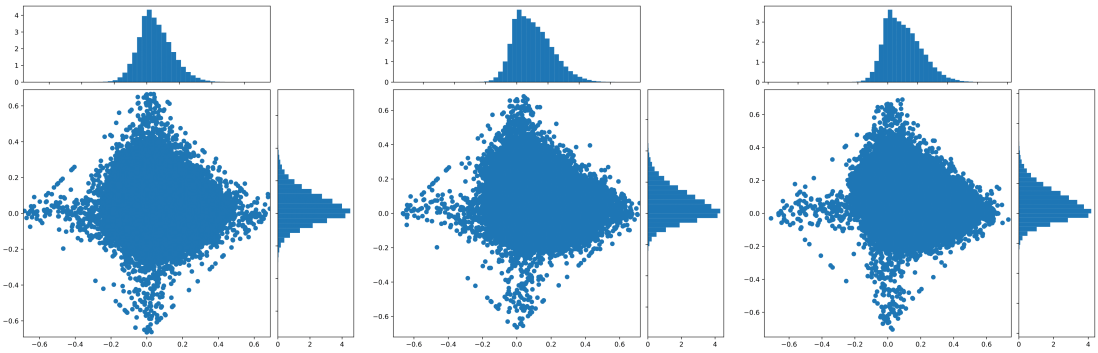

(A) $\beta = 0.5$ (B) $\beta = 2$ (C) $\beta = 6$

FIGURE 12. One and two dimensional velocity histograms for $N = 900$ obstacles. Parameters: $\alpha = 0$, $\lambda = 1$, $\sigma = 0.2$, $\beta = 0.5$ (12a), $\beta = 2$ (12b), $\beta = 6$ (12c).

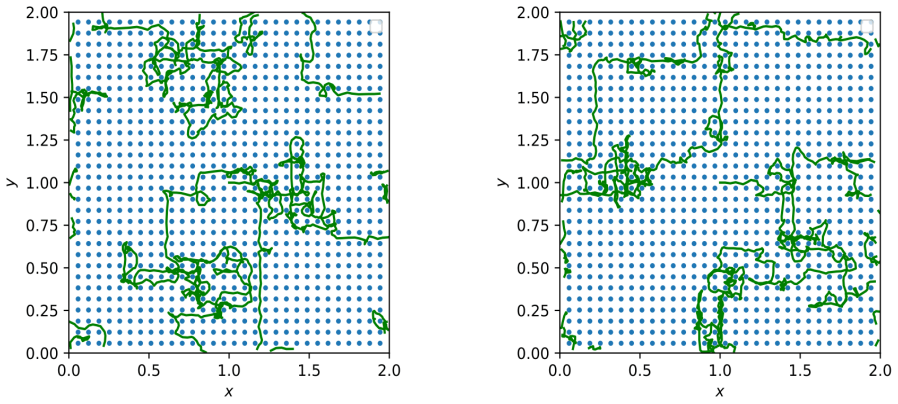

(A) $\beta = 0.5$ (B) $\beta = 6$

FIGURE 13. Particle's trajectories for $N = 900$ obstacles. Parameters: $\alpha = 0$, $\lambda = 1$, $\sigma = 0.2$, $\beta = 0.5$ (13a) and $\beta = 6$ (13b).

$\beta = 0.5$, this behaviour is more remarkable. As β increases, the velocity distribution becomes more concentrated towards parts of the domain different from the half-upper-right side. This is due to the fact that the force intensity is less efficient on the particle's dynamics because now the particle feels also its own internal dynamics. Figure 16 shows two particle's trajectories for $N = 900$ obstacles, for $\beta = 0.5$ (Figure 16a) and $\beta = 6$ (Figure 16b). We notice that for $\beta = 0.5$, the particle's trajectories mainly covers the upper part of the domain. For $\beta = 6$, we can recognize some persistence directions in agreement with the direction of the force, but they are also very perturbed. Indeed, since $\alpha > 0$ and big enough, the particle's dynamics feels the competition between the force intensity and its own internal dynamics. For this reason, the particle may cover different directions with respect to that induced by the constant force. This is in agreement with the velocity histogram in Figure (15c).

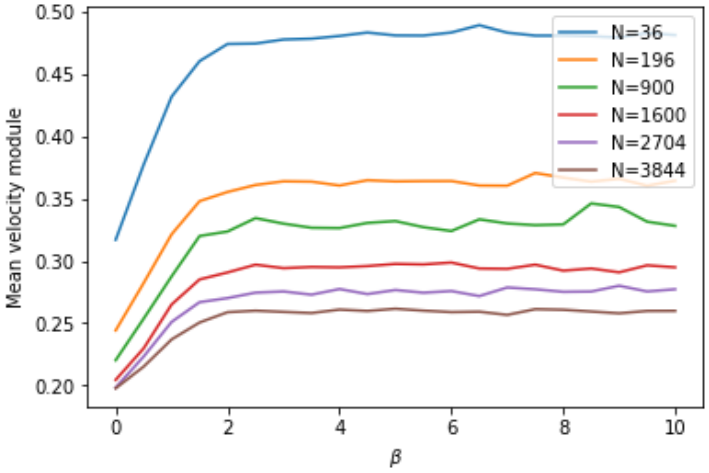

FIGURE 14. Mean velocity modulus among $M = 100$ simulations. We set $\alpha = 30$, $\lambda = 1$, $\sigma = 0.2$ and we simulated for 20 values of $\beta \in [0, 10]$. Numbers of obstacles considered: $36, 196, 900, 1600, 2704, 3844$.

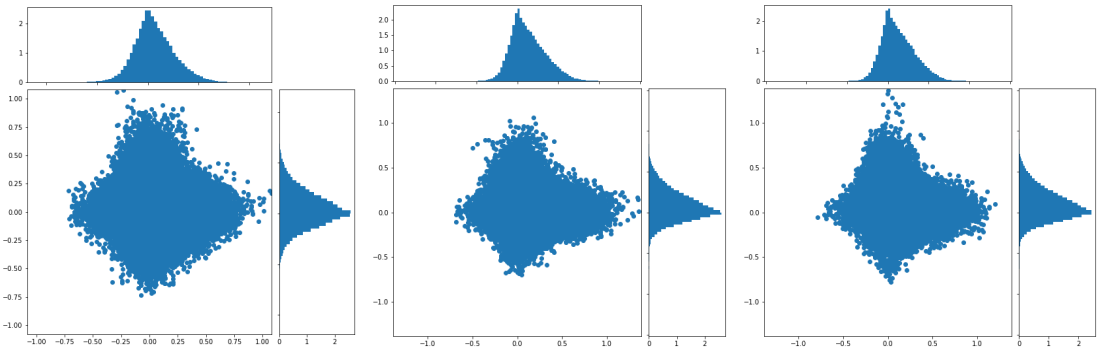

(A) $\beta = 0.5$ (B) $\beta = 2$ (C) $\beta = 6$

FIGURE 15. One and two dimensional velocity histograms for $N = 900$ obstacles. Parameters: $\alpha = 30$, $\lambda = 1$, $\sigma = 0.2$, $\beta = 0.5$ (15a), $\beta = 2$ (15b), $\beta = 6$ (15c).

CONCLUSION

In the present proceeding, we studied the effects of some particular biochemical and mechanical cues on cell migration. In the first part, we introduced a two dimensional continuous stochastic model to describe the effects of biochemical cues on cell migration. This continuous model relies on biological assumptions. More precisely we considered the dynamics of a cell in the presence of a constant gradient of attractive signal. With this model we wanted to study the competition between the internal cell's dynamics and the intensity of the signal. In the one dimensional case, we obtained an explicit formulation of the stationary velocity distribution. We noticed that when the signal intensity is weak, the cell moves according to its internal dynamics. If instead the signal intensity is strong enough, the cell follows the signal.

In the second part, we numerically investigated the combined effects of obstacles and of a constant directional force on the cell's dynamics for a cell described as an active particle. We first considered

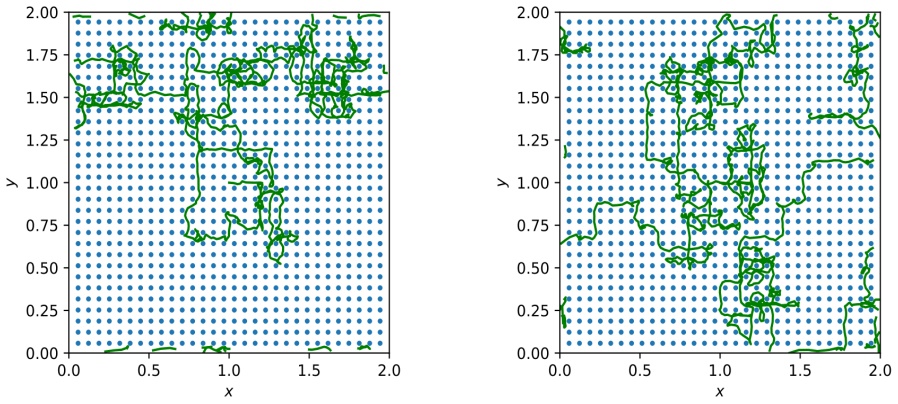

(A) $\beta = 0.5$ (B) $\beta = 6$

FIGURE 16. Particle's trajectories for $N = 900$ obstacles. Parameters: $\alpha = 30$, $\lambda = 1$, $\sigma = 0.2$, $\beta = 0.5$ (16a) and $\beta = 6$ (16b).

a damped Brownian particle in a crowded environment and without external signal. For this case, by analysing the two dimensional velocity histograms, we noticed that the presence of obstacles has an effect on the directionality of the particle, which becomes stronger as the number of obstacles increases and as the damped effect decreases. Then, we studied the additional effect of a constant directional force. We noticed that the mean velocity modulus increases as the force intensity increases until it reaches a limit value. Moreover, we saw that the mean velocity modulus decreases as the number of obstacles increases, but this does not change its qualitative behaviour. We analysed also the two dimensional velocity histograms. We first noticed that the one dimensional histograms show an asymmetry towards positive values which becomes more evident as the force intensity increases. Furthermore, the two dimensional velocity distribution seems to be more concentrated in the direction of the external constant force. This behaviour becomes more remarkable as the force intensity increases. Finally, we considered an active particle whose dynamics is also characterized by an internal dynamics in a crowded environment and with an external signal. We noticed that the mean velocity modulus does not change qualitatively with respect to the previous case. As for the two dimensional histograms, we noticed that the velocity distribution is not only concentrated in the direction of the external constant force, but also in other regions of the domain. This different behaviour is due to the presence of the internal dynamics. We can thus observe that the presence of the obstacles has an effect on the directional behaviour of the particle's dynamics. Indeed, the presence of the obstacles enforces the particle to move towards particular regions of the domain. The presence of an external constant force enforces the particle to move in the direction of the force. Furthermore, the internal dynamics enforces the persistence induced by the presence of the obstacles as well as the by external constant force.

ACKNOWLEDGEMENT

The present research was carried out within the scope of the 2018 CEMRACS Summer Program. The authors acknowledge support from SMAI (French Society of Applied and Industrial Mathematics), PEPS MI from CNRS and from the MESOPROBIO ERC. The authors would like to take the opportunity to thank the organizing committee of this even for giving us the chance to join Cemracs 2018, as well as Sepideh Mirrahimi for her support on this project.

References

[1] R. Ananthakrishnan and A. Ehrlicher. The forces behind cell movement. International journal of biological sciences, 3:303–17, 2007.

[2] O. Barreiro, P. Martín, F. Sánchez-Madrid, and R. González-Amaro. Molecular cues guiding inflammatory responses. Cardiovascular Research, 86(2):174–182, 2010.

[3] U. Basu and C. Maes. Mobility transition in a dynamic environment. Journal of Physics A: Mathematical and Theoretical, 47(25):255003, 2014.

[4] O. Bénichou, P. Illien, G. Oshanin, A. Sarracino, and R. Voituriez. Nonlinear response and emerging nonequilibrium microstructures for biased diffusion in confined crowded environments. Phys. Rev. E, 93:032128, 2016.

[5] P. Ciarlet. Introduction à l'analyse numérique matricielle et à l'optimisation. Masson, Paris, 1990.

[6] P. N. Devreotes and S. H. Zigmond. Chemotaxis in eukaryotic cells: A focus on leukocytes and dictyostelium. Annual Review of Cell Biology, 4(1):649–686, 1988. PMID: 2848555.

[7] C. Etchegaray. Mathematical and numerical modelling of cell migration. Thesis, Université Paris-Saclay, 2016.

[8] C. Etchegaray and N. Meunier. Crawling migration under chemical signalling: A stochastic model. Mathematical Methods in the Applied Sciences, 41(18):8799–8815, 2018.

[9] C. Etchegaray and N. Meunier. A stochastic model for protrusion activity. ESAIM: Proceedings, 62:56–67, 2018.

[10] C. Etchegaray, N. Meunier, and R. Voituriez. A 2d deterministic model for single-cell crawling, a minimal multiscale approach. submitted for publication, pages 1385–405.

[11] C. Etchegaray, N. Meunier, and R. Voituriez. Analysis of a nonlocal and nonlinear fokker-planck model for cell crawling migration. SIAM Journal on Applied Mathematics, 77(6):2040–2065, 2017.

[12] N. Fournier and S. Meleard. A microscopic probabilistic description of a locally regulated population and macroscopic approximations. Annals of Applied Probability, 14, 2004.

[13] C. Grabher, A. Cliffe, K. Miura, J. Hayflick, R. Pepperkok, P. Rørth, and J. Wittbrodt. Birth and life of tissue macrophages and their migration in embryogenesis and inflammation in medaka. Journal of leukocyte biology, 81:263–71, 2007.

[14] D. J. Higham. An algorithmic introduction to numerical simulation of stochastic differential equations. SIAM Rev., 43(3):525–546, 2001.

[15] A. Lefebvre and A. Lefebvre-Lepot. Numerical modelling of fluid/particle flows. Theses, Université Paris Sud - Paris XI, 2007.

[16] A. Lodish and S. Zipursky. Molecular cell biology. Biochemestry and Molecular Biology Education, 29:126–33, 2001.

[17] B. Maury. A time-stepping scheme for inelastic collisions. Numerische Mathematik, 102(4):649–679, 2006.

[18] B. Maury and J. Venel. A discrete contact model for crowd motion. ESAIM: Mathematical Modelling and Numerical Analysis, 45(1):145–168, 2011.

[19] S. Mcdougall, J. Dallon, J. Sherratt, and P. Maini. Fibroblast migration and collagen deposition during dermal wound healing: Mathematical modelling and clinical implications. Philosophical transactions. Series A, Mathematical, physical, and engineering sciences, 364:1385–405, 2006.